Experimental and Theoretical Reaction Cross Sections for the H + HCl System†

F. J. Aoiz,‡ L. Bañares,‡ T. Bohm,§ A. Hanf,§ V. J. Herrero,|| K.-H. Jung,⊥ A. Läuter,§ K. W. Lee,⊥ M. Menéndez,‡ V. Sáez Rábanos,# I. Tanarro,|| H.-R. Volpp,*,§ and J. Wolfrum§

Departamento de Química Física, Facultad de Química, Universidad Complutense, 28940 Madrid, Spain, Physikalisch-Chemisches Institut der Universität Heidelberg, Im Neuenheimer Feld 253, D-69120 Heidelberg, Germany, Instituto de Estructura de la Materia (CSIC), Serrano 123, 28006 Madrid, Spain, Department of Chemistry and School of Molecular Science (BK21), Korea Advanced Institute of Science and Technology, Taeduck Science Town, Taejon 305-701, Korea, and Departamento de Química General y Bioquímica, ETSI de Montes, Universidad Politécnica, 28040 Madrid, Spain

Received: April 24, 2000; In Final Form: July 11, 2000

The dynamics of the gas-phase reaction of H atoms with HCl has been studied experimentally employing the laser photolysis/vacuum-UV laser-induced fluorescence (LP/VUV-LIF) "pump-and-probe" technique and theoretically by means of quasiclassical trajectory (QCT) calculations performed on two versions of the new potential energy surface of Bian and Werner [Bian, W.; Werner, H.-J. *J. Chem. Phys*. **2000**, *112*, 220]. In the experimental studies translationally energetic H atoms with average collision energies of E_{col} = 1.4 and 1.7 eV were generated by pulsed laser photolysis of H_2S and HBr at 222 nm, respectively. Ground-state Cl($^2P_{3/2}$) and spin−orbit excited Cl*($^2P_{1/2}$) atoms produced in the reactive collision of the H atoms with room-temperature HCl were detected under single collision conditions by VUV-LIF. The measurements of the Cl* formation spin−orbit branching ratio ϕ_{Cl^*}(1.4 eV) = [Cl*]/[Cl + Cl*] = 0.07 ± 0.01 and ϕ_{Cl^*}(1.7 eV) = 0.19 ± 0.02 revealed the increasing importance of the nonadiabatic reaction channel H + HCl → H_2 + Cl* with increasing collision energy. To allow for comparison with the QCT calculations, total absolute reaction cross sections for chlorine atom formation, σ_R(1.4 eV) = (0.35 ± 0.16) Å^2 and σ_R(1.7 eV) = (0.13 ± 0.06) Å^2, have been measured using a photolytic calibration method. In addition, further QCT calculations have been carried out for the H + DCl isotope reaction which can be compared with the results of previous reaction dynamics experiments of Barclay et al. [Barclay, V. J.; Collings, B. A.; Polanyi, J. C.; Wang, J. H. *J. Phys. Chem.* **1991**, *95*, 2921].

I. Introduction

The gas-phase reaction of hydrogen atoms with hydrogen chloride and the corresponding reverse reaction of chlorine atoms with molecular hydrogen represent important elementary steps in the $H_2 + Cl_2 = 2HCl$ reaction system which has played a major role in the development of chemical kinetics.[1] The experimental work of Bodenstein and Dux[2,3] eventually established for that system the presence of a chain mechanism in which Cl atoms act as chain carriers.[4] Since then a large number of kinetics studies were carried out for the H + HCl elementary reaction in the temperature range 195 K ≤ T ≤ 1200 K[5] including experiments in which the influence of selective vibrational excitation of HCl on the reaction rate was investigated.[6−8] The kinetics of the Cl + H_2 reaction was also studied in great detail over a wide range of temperatures 199 K ≤ T ≤ 3020 K and the experimental rate constants[5d,9] were found to be in general good agreement with the results of rate constant calculations[10−12] on the G3 potential energy surface (PES),[13] although in the lower temperature region (199 K ≤ T ≤ 600 K), the calculated rate constants tended to be too high.

In addition to the kinetics studies a number of detailed experimental studies on the dynamics of the Cl + H_2/D_2/HD reaction employing translational and spin−orbit excited Cl atoms as well as rotational and vibrational state selected H_2, D_2, and HD reagents, respectively, were reported recently.[14−16] The HCl angular distributions and time-of-flight spectra measured by Casavecchia and co-workers for different laboratory scattering angles for the Cl + H_2(v = 0) reaction at an reagent collision energy of E_{col} = 0.25 eV could be well reproduced by quantum mechanical (QM) scattering and quasiclassical trajectory (QCT) calculations performed on the G3 PES.[14] On the other hand, isotopic branching ratios measured for the H + DCl and D + HCl product channels of the Cl + HD reaction could not be reproduced by QM reactive scattering calculations performed on the G3 PES.[17] Whereas the measured relative excitation functions, $\sigma_R(E_{col})$, obtained in the collision energy range E_{col} = 0.17−0.35 eV, revealed a marked preference for H + DCl product channel, QM calculations on the G3 PES predicted the formation of HCl or DCl to occur with almost equal probability. On the contrary, QM calculations on a new PES constructed by Bian and Werner[18] yielded an almost perfect agreement with the experimental DCl/HCl product branching ratios.[17]

Due to the relatively low collision energies employed in the Cl + H_2 dynamics experiments these studies provided detailed

† Part of the special issue "C. Bradley Moore Festschrift".

* Corresponding author. E-mail: aw2@ix.urz.uni-heidelberg.de.

‡ Departamento de Química Física, Facultad de Química, Universidad Complutense.

§ Physikalisch-Chemisches Institut der Universität Heidelberg.

|| Instituto de Estructura de la Materia (CSIC).

⊥ Department of Chemistry and School of Molecular Science (BK21), Korea Advanced Institute of Science and Technology.

Departamento de Química General y Bioquímica, ETSI de Montes, Universidad Politécnica

10.1021/jp001555j CCC: $19.00
Published on Web 09/01/2000

information about the region of the HClH−PES close to the threshold of reaction. However, much less information is available concerning the high-energy regions of the PES which can be assessed in H + HCl dynamics experiments using translationally excited H atoms.[19−22] For the H + HCl reaction the following product channels can be distinct:

$$H + HCl \rightarrow H_2 + Cl(^2P_{3/2}) \quad \Delta H_0 = -0.045 \text{ eV} \quad (1a)$$

$$H + HCl \rightarrow H_2 + Cl^*(^2P_{1/2}) \quad \Delta H_0 = 0.065 \text{ eV} \quad (1b)$$

$$H + HCl \rightarrow HCl + H \quad (2)$$

Reaction channels 1a and 1b represent adiabatic and nonadiabatic H-atom abstraction channels, respectively, while reaction channel 2 represents the H-atom exchange channel.

So far there have been only two measurements of total absolute reaction cross sections for the abstraction reaction 1. In ref 22, a value of $\sigma_R(1.0 \text{ eV}) = (0.34 \pm 0.05)$ Å^2 was determined employing vacuum-UV laser-induced fluorescence (VUV-LIF) for Cl($^2P_{3/2}$) atom detection. Valentini and co-workers determined a value of (2 ± 1) Å^2 at $E_{col} = 1.6$ eV using coherent anti-Stokes Raman scattering (CARS) spectroscopy for H_2 product detection.[20] Although the latter result suggests a pronounced increase of the abstraction reaction cross section with increasing collision energy, such a pronounced increase could, however, not be reproduced in QCT calculations on the G3 PES.[23] Furthermore, a sharp increase in the H + HCl abstraction reaction cross section by a factor of ∼6 in the range $E_{col} = 1.0-1.6$ eV would be at variance with reaction cross sections determined by Polanyi and co-workers who observed that for the H + DCl reaction the abstraction cross section decreases with increasing collision energy from a value of 0.2 Å^2 at $E_{col} = 1.2$ eV to a value of 0.1 Å^2 at $E_{col} = 1.8$ eV.[21] An attempt to observe spin−orbit excited Cl* atoms formed via the nonadiabatic abstraction reaction channel (eq 1b) was also reported.[22] However, only an upper limit for the cross section for Cl* formation at a collision energy of $E_{col} = 1.0$ eV could be obtained in this study.

The aim of the present study was to investigate the collision energy dependence of the reaction cross section of reaction 1 for $E_{col} > 1.0$ eV both experimentally by absolute reaction cross section measurements and theoretically by means of quasiclassical trajectory (QCT) calculations performed on two versions (termed as BW1 and BW2) of the new potential energy surface of Bian and Werner.[18] To the best of our knowledge, no dynamical calculations for the H + HCl and the H + DCl reaction systems corresponding to the high-collision-energy region were reported so far for the BW1 or BW2 PESs. In addition, we report about experiments carried out to characterize the nonadiabatic reaction channel (eq 1b) and its collision-energy dependence.

II. Experiment

The experimental studies were carried out in a flowing mixture of H_2S (UCAR electronic grade) and HBr (Messer Griesheim, 99.8%), respectively, with room-temperature HCl (Messer Griesheim, 99.999%). The ratios of [H_2S]:[HCl] and [HBr]:[HCl] were typically 1:2 at a total pressure between 60 and 90 mTorr. The experiments were performed in a flow reactor apparatus similar to the one used in our previous H + HCl reaction dynamics studies at $E_{col} = 1.0$ eV.[22] For the Cl atom photolytic calibration measurements PCl_3 (Aldrich, 99.99%) was flowed through the flow reactor at pressures of typically 1−2 mTorr. PCl_3 was degassed prior to use by freeze−pump−thaw cycles.

An excimer laser operating with a KrCl gas mixture ($\lambda_{pump} = 222$ nm) with a spectral bandwidth of ∼80 cm^{-1} and a pulse duration of 15−20 ns was used to photodissociate the H atom precursor molecules H_2S and HBr, respectively, to generate translationally energetic H atoms with average collision energies of $E_{col} = 1.4$ eV[24] and $E_{col} = 1.7$ eV[25,26] in the (H−HCl)-center-of-mass system with an energy spread of about 10%.[27] Pump laser intensities employed in the experiments were in the range 2−5 mJ/cm^2.

Pulsed narrow-band VUV-probe laser radiation (pulse duration 10−15 ns; bandwidth $\Delta\omega_{probe} = 0.4$ cm^{-1}), tunable in the wavelength region 133.5−136.4 nm, was generated using the Wallenstein method for resonant third-order sum−difference frequency conversion ($\omega_{probe} = 2\omega_R - \omega_T$) of pulsed dye laser radiation in krypton.[28] In the four-wave mixing process the frequency ω_R ($\lambda_R = 212.55$ nm) is two-photon resonant with the Kr 4p−5p (1/2, 0) transition. The frequency ω_T could be tuned from 480 to 521 nm to cover the four allowed Cl($4s^2P_{j'} \leftarrow 3p^2P_{j''}$; j' = 1/2, 3/2 ← j'' = 1/2, 3/2) transitions.[29] Ground-state Cl($^2P_{3/2}$) and spin−orbit excited-state Cl*($^2P_{1/2}$) atoms ($\Delta E_{so} = E(^2P_{1/2}) - E(^2P_{3/2}) = 881$ cm^{-1}) were detected using the (j' = j'')-transitions, which have the highest transition probabilities $f_{3/2,3/2} = 0.114$ and $f_{1/2,1/2} = 0.088$, respectively.[30]

The fundamental laser radiation was obtained from two tunable dye lasers, simultaneously pumped by a XeCl excimer laser, one of which, ω_R, was frequency doubled with a BBO II crystal. The generated VUV-light was carefully separated from the fundamental laser radiation by a lens monochromator. The probe beam was aligned to overlap the photolysis beam at right angles in the viewing region of a LIF detector. The delay time between the photolysis and probe pulse was controlled by a pulse generator and could be monitored on a fast oscilloscope. Delay times between pump and probe laser pulses were typically between $\Delta t = (100 \pm 5)$ ns and $\Delta t = (250 \pm 5)$ ns allowing the collision-free detection of the nascent Cl and Cl* atoms produced in the reaction. Under these experimental conditions relaxation of Cl* by quenching was negligible. The Cl and Cl* LIF signals were measured through a band-pass filter (ARC model 130-B-1D with a transmission 29% at 134 nm) by a solar blind photomultiplier (THORN EMI model 9413 B) positioned at right angles to both pump and probe laser. The VUV-probe beam intensity was monitored after passing through the reaction cell with an additional solar blind photomultiplier of the same type. To obtain a satisfactory *S*/*N* ratio, each point of the Cl and Cl* atom Doppler profiles shown in Figure 1 were typically averaged over 30 laser shots. Experiments were carried out at a laser repetition rate of 6 Hz. The Cl and Cl* LIF signals, VUV probe beam and pump laser intensity were recorded with a boxcar system and transferred to a microcomputer where the LIF signal was normalized to both pump and probe laser intensities.

It was found that the VUV probe beam itself produced an appreciable Cl/Cl* atom LIF signal via photolysis of HCl and PCl_3, respectively. To subtract these "background" Cl/Cl* atoms from the Cl/Cl* atoms produced in the H + HCl reaction and in the 222 nm photolysis of PCl_3 an electronically controlled mechanical shutter was inserted into the pump laser beam path (see Figure 1 of ref 22). At each point of the Cl and Cl* atom line scan, the signal was first averaged with the shutter opened and again averaged with the shutter closed. A point-by-point

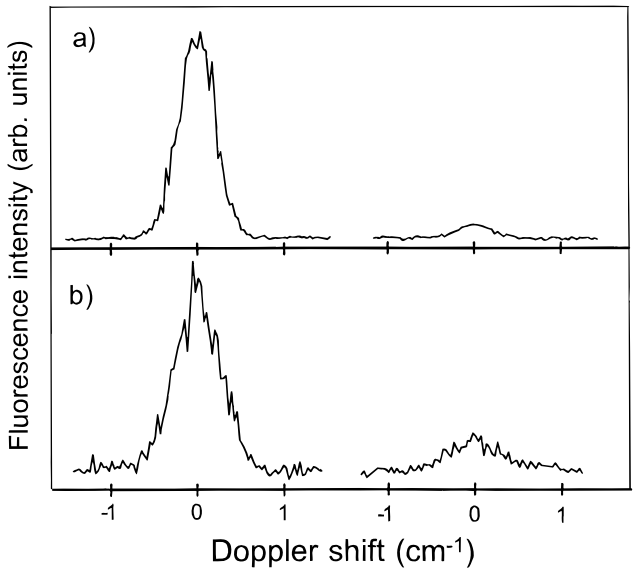

Figure 1. (a) Doppler profiles of Cl (left-hand side) and Cl* (right-hand side) product atoms observed in the 222 nm photolysis of a 1:2 mixture of H_2S and HCl (p_{tot} = 70 mTorr; Δt = 180 ns). (b) Doppler profiles of Cl (left-hand side) and Cl* (right-hand side) product atoms observed in the 222 nm photolysis of a 1:2 mixture of HBr and HCl (p_{tot} = 85 mTorr; Δt = 150 ns). Line centers correspond to the ($4s^2P_{j'=3/2} \leftarrow 3p^2P_{j''=3/2}$) transition of the Cl atom (74225.8 cm^{-1}) and to the ($4s^2P_{j'=1/2} \leftarrow 3p^2P_{j''=1/2}$) transition of the Cl* atom (73983.1 cm^{-1}), respectively.

subtraction procedure was adopted,[22] to obtain directly and on-line a signal free from "probe-laser-generated" background Cl and Cl* atoms.

Although the Cl* atom product signals were considerably smaller than the Cl atom product signals, measurements in which Cl* Doppler profiles were recorded at different pump−probe delay times in the range Δt = 100−250 ns confirmed the linear increase of the Cl* product concentration with pump−probe delay time, $[Cl^*] \propto \sigma_R^* \, v_{rel} \, \Delta t$, which is expected if Cl* is formed by the reaction of energetic H atoms with HCl under single-collision conditions.[22]

III. Theoretical Method

The method for the calculation of the quasiclassical trajectories has been described elsewhere[11,23,31] and therefore only specific details, relevant for the present study, are given in the following.

QCT calculations for H + HCl(v = 0) and H + DCl(v = 0) were carried out on the new PES of Bian and Werner.[18] This PES, which is based on extensive and high quality ab initio calculations (1200 geometries were used as compared with the 87 points for the G3 PES[13]), has been released in two slightly different versions termed BW1 and BW2, respectively. The BW1 version is based on a fit of the actual ab initio points, whereas the BW2 version was computed by scaling the correlation energies at all geometries with a constant factor chosen in order to reproduce more accurately the dissociation energies of HCl and H_2. The transition state for the abstraction channel is very similar in the BW1, BW2, and G3 PESs; in the three cases, the minimum energy barrier corresponds to a collinear configuration and the heights of the respective classical barriers are 0.200, 0.184, and 0.194 eV. No spin−orbit corrections were included at any stage of the dynamical treatment. Calculations were performed for the two reaction channels − abstraction (1) and exchange (2) − of each isotopic variant for an interval of collision energies [E_1, E_2]. The upper limit, E_2, of this energy interval was in all cases set equal to 2.5 eV. To determine the E_1 value and to make a pre-selection of the range of impact parameters relevant for reaction, an auxiliary line-of-centers excitation function with a slightly lower threshold (E_1) and somewhat larger cross sections than those of the actual reaction was constructed for each case with a reduced number of trajectories following the procedure indicated in refs 11 and 23.

The initial rotational state, j, of the HCl/DCl molecule was sampled with the weight corresponding to a thermal distribution at a given temperature. With an appropriate re-weighting of a single set of trajectories one can obtain not only an averaged $\sigma_R(E_{col})$, for a given rotational temperature and initial HCl/DCl vibrational state, but also an excitation function for each initial rovibrational state. The integration step size in the trajectories was chosen to be 5×10^{-17} s, and the initial distance where the trajectories were started was 8 Å. This guarantees a conservation of the total energy better than 1 in 10^5 and 1 in 10^7 in the total angular momentum. The rovibrational energies of HCl and DCl were calculated by semiclassical quantization of the classical action using in each case the asymptotic diatomic potential of the PES (see ref 11 and references therein).

A batch of 200 000 trajectories was calculated at T = 300 K for each of the surfaces, BW1 and BW2, investigated. The thermally averaged reaction cross sections $\sigma_R(E_{col})$ and $\sigma_R(E_{col}: v, j)$ values for each initial HCl(v, j) rovibrational state were subsequently calculated by the method of moment expansion in Legendre polynomials, as described in detail in ref 11. Significance levels higher than 95% could be achieved by using 5−10 Legendre moments, ensuring a very good convergence such that the inclusion of more terms does not produce any significant change. The error bars were calculated as in ref 11 and correspond to $\pm 1\sigma$.

IV. Results and Discussion

(a) Experimental Chlorine Atom Spin−Orbit Branching Ratio. Figure 1a shows typical Doppler profiles of ($^2P_{3/2}$) ground-state Cl atoms (left-hand side) and ($^2P_{1/2}$) spin−orbit excited Cl* atoms (right-hand side) produced in the H + HCl reaction at E_{col} = 1.4 eV. In Figure 1b, Doppler profiles of Cl (left-hand side) and Cl* atoms (right-hand side) produced in the H + HCl reaction at E_{col} = 1.7 eV are depicted. Spin−orbit branching ratios, $\phi_{Cl^*}(1.4\ eV) = [Cl^*]/[Cl + Cl^*] = 0.07 \pm 0.01$ and $\phi_{Cl^*}(1.7\ eV) = 0.19 \pm 0.02$, for Cl* atom product formation were determined from the integrated areas of the corresponding Doppler profiles recorded for the two different collision energies after correcting for the different oscillator strengths of the spectral transitions used to probe the two different fine-structure states. The quoted error represents the $\pm 1\sigma$ statistical uncertainties obtained in the evaluation of the experimental data (for each collision energy about 15 sets of Cl and Cl* Doppler profiles were evaluated).

In Figure 2, the Cl* branching ratio values obtained in the present work are plotted against the collision energy. For comparison the branching ratio for Cl* atom product formation obtained in ref 22 at E_{col} = 1.0 eV is also included. The present measurements clearly indicate that the relative contribution of the nonadiabatic abstraction reaction channel H + HCl → H_2 + Cl* (eq 1b) increases with increasing collision energy. In a previous dynamics study of the H + DCl reaction no Cl* product signals could be observed.[21] The upper limit of the Cl* formation cross sections reported in ref 21 for the H + DCl → HD + Cl* product channel corresponds to $\phi_{Cl^*} \approx 0.1$ in the collision energy range E_{col} = 1.2−1.8 eV.

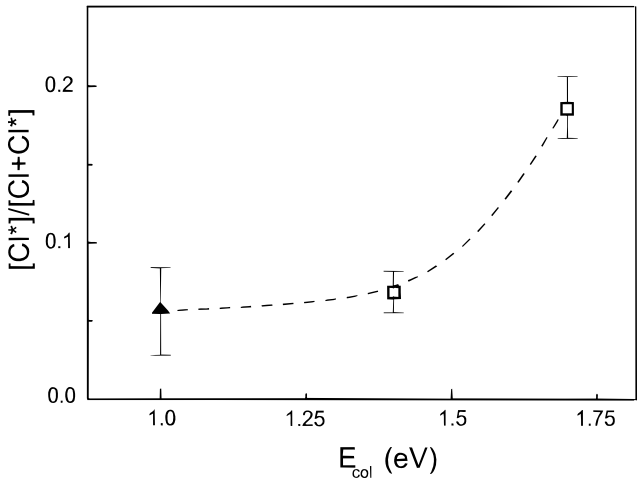

Figure 2. Dependence of the measured Cl* atom spin−orbit branching ratio [Cl*]/[Cl + Cl*] on the H + HCl reagent collision energy. The solid triangle represents the results of ref 22. The open squares are the results of the present study. The dashed line is drawn just to guide the eye.

The present observation of Cl* product formation in the H + HCl reaction is closely related to the recent work of Liu and co-workers on the corresponding back reaction Cl* + H_2 → H + HCl (eq −1b).[15b] In these studies it was found that at a collision energy of $E_{col} = 0.23$ eV, Cl* atoms are by a factor of ∼6 more reactive to H_2 than ground-state Cl atoms. The reactivity of the Cl* reagents toward H_2 was attributed to nonadiabatic transitions from the initially populated nonreactive (2^2A')-PES to the ground (1^2A')-PES which correlates with H + HCl ground-state products. It was postulated that these nonadiabatic transitions take place predominately near the avoided-crossing region at bent Cl−HH geometries in the Cl + H_2 entrance channel.

The Cl* product formation in the H + HCl reaction and its collision-energy dependence as observed in the present experiments can be rationalized in the framework of the above mechanism. For the H + HCl abstraction reaction 1, it has been shown that for low collision energies, $E_{col} \approx 0.7$ eV, the products are scattered almost exclusively into the backward hemisphere indicating a direct rebound-type mechanism.[32] The restriction to collinear H−HCl approach geometries at low collision energies was attributed to the strongly repulsive H−H−Cl bending potential which leads to a sharp increase of the reaction barrier height for approach geometries deviating from the collinear one. For higher collision energies, $E_{col} \approx 1.6$ eV, however, significant contributions due to noncollinear reactive collisions became noticeable. Hence, the sharp increase in the Cl* spin−orbit branching ratio (see Figure 2) with increasing collision energy could be explained by an increase in the reaction probability for noncollinear reagent geometries at higher collision energies which could promote the occurrence of nonadiabatic transitions between the (1^2A') H−HCl−PES − which correlates with H_2 + Cl products − and the (2^2A')-PES − which correlates with H_2 + Cl* products − in the exit channel of the H + HCl abstraction reaction pathway. However, for a quantitative description of the nonadiabatic interactions which govern the formation of Cl* atoms in the H + HCl reaction, multi-surface scattering calculations which take into account all relevant couplings are clearly needed.[33]

In the following section, results of total reaction cross section measurements for the H + HCl abstraction reaction 1 will be reported which allow for comparison with the results of

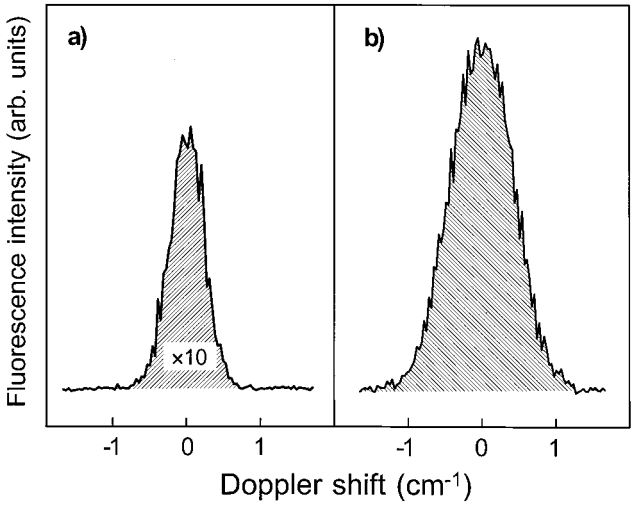

Figure 3. Doppler profiles of (a) Cl atoms produced in the reaction H + HCl (experimental conditions:1:2 mixture of H_2S and HCl; p_{tot} = 70 mTorr; Δt = 180 ns), (b) Cl atoms produced in the photolysis of 1.5 mTorr PCl_3 at 222 nm. Line centers correspond to the ($4s^2P_{j'=3/2} \leftarrow 3p^2P_{j''=3/2}$) transition of the Cl atom (74225.8 cm^{-1}). Details about the photolytic calibration method for the determination of absolute reaction cross sections are given in the text.

dynamical simulations employing available (1^2A') adiabatic H−HCl−PESs (see section IV(c)).

(b) H + HCl → H_2 + Cl/Cl* Reaction Cross Sections. The total absolute reaction cross section for the H + HCl → H_2 + Cl/Cl* abstraction reaction (eq 1) was obtained by means of a photolytic calibration method using pulsed laser flash photolysis of PCl_3 as a reference source of well-defined Cl atom concentrations. Following the photolytic calibration procedure introduced in ref 22, the total absolute reaction cross section σ_R(1.4 eV) for the H + HCl abstraction reaction 1 for example can be obtained by comparing the Cl atom signal, S_{Cl}(H + HCl)− defined as the area below the Cl atom Doppler profile in Figure 3a−produced in the reaction of H atoms generated by the 222 nm photolysis of H_2S with HCl, with the Cl atom signal S_{Cl}-(PCl_3) produced in the 222 nm photolysis of PCl_3 (Figure 3b) via the following formula:

$$\sigma_R(1.4\text{ eV}) = \frac{S_{Cl}(H + HCl)}{S_{Cl}(PCl_3)} \cdot \frac{\phi_{Cl}(PCl_3)}{\phi_{Cl}(H + HCl)} \cdot \frac{\sigma(PCl_3)}{\sigma(H_2S)} \cdot \frac{[PCl_3]}{[H_2S][HCl]} \cdot \frac{\Phi_{Cl+Cl^*}(PCl_3)}{v_{rel}\Delta t} \quad (3)$$

In eq 3, v_{rel} is the relative velocity which corresponds to the average translational energy of $E_{col} = 1.4$ eV of the H + HCl reactant pair and Δt is the time delay between the pump and probe laser pulses. [X] denotes the gas-phase concentration of species X calculated from the corresponding partial pressures. $\phi_{Cl}(PCl_3)$ stands for the Cl atom spin−orbit branching ratio [Cl]/[Cl + Cl*] = 0.47 ± 0.05 and $\Phi_{Cl+Cl^*} = 0.76 \pm 0.13$ is the total chlorine atom quantum yield. Both quantities have been determined in recent photodissociation dynamics studies of PCl_3 after UV excitation at 222 nm.[34] ϕ_{Cl}(H + HCl) is the Cl atom spin−orbit branching ratio [Cl]/[Cl + Cl*] = 0.93 ± 0.01 obtained in the H + HCl reaction measurement. $\sigma(PCl_3)/\sigma(H_2S)$ represents the ratio of the PCl_3 and H_2S optical absorption cross sections at 222 nm. A value of $\sigma(PCl_3)/\sigma(H_2S) = 11.3 \pm 1.7$ was determined in the present study which is in good agreement with the value of 11.5 which can be calculated from the corresponding literature values $\sigma(PCl_3) = 1.2 \times 10^{-17}$ cm^2 [35] and $\sigma(H_2S) = 1.04 \times 10^{-18}$ cm^2.[36]

To determine the total absolute reactive cross section for the H + HCl abstraction reaction 1 in a number of experimental runs, integrated areas under the Cl fluorescence excitation spectra were determined for identical experimental conditions and evaluated using eq 3. Forty calibration measurements yielded an average value for the H + HCl abstraction reaction cross section of $\sigma_R(1.4\ \text{eV}) = (0.35 \pm 0.16)$ Å^2. A similar calibration procedure in which HBr photolysis at 222 nm was employed to generate translationally excited H atom reagents with $E_{col} = 1.7$ eV yielded a value of $\sigma_R(1.7\ \text{eV}) = (0.13 \pm 0.06)$ Å^2. The quoted experimental errors were calculated from the individual errors of the entries of formula 3 on the basis of simple error propagation.

The present results clearly indicate that there is no sharp increase in the H + HCl abstraction reaction cross section for $E_{col} > 1.0$ eV. The finding that the abstraction reaction cross section decreases at higher collision energies ($E_{col} > 1.4$ eV) is in agreement with the decrease in the H + DCl → HD + Cl abstraction reaction cross section observed by Polanyi and co-workers in the energy range $E_{col} = 1.2-1.8$ eV.[21]

In the following section, the present results of the total abstraction cross section measurements and the previous results for the H + DCl reaction[21] will be compared with results of QCT calculations carried out on the G3, BW1, and BW2 PESs.

(c) Theoretical Reaction Cross Sections for the H + HCl/DCl Reactions. The QCT excitation functions for the abstraction channel (eq 1) of the H + HCl reaction are shown in the upper panel of Figure 4. To allow for comparison with the experiments for the whole range of collision energies considered, the displayed cross sections correspond to a $T = 300$ K distribution of HCl reagent rotational levels in the ground vibrational state. Excitation functions for individual rotational levels $\sigma_R(E_{col}$:v $= 0, j)$ were also obtained in the $j = 0-6$ interval, but no appreciable dependence of the cross section on j was observed (as in the calculations on the G3 PES of ref 11) and they are not shown. As can be seen in Figure 4, for the two BW PESs the cross sections raise from threshold ($E_0 \approx 0.15$ eV) to a nearly constant value of 0.5−0.6 Å^2 for $E_{col} > 1.0$ eV. The QCT cross sections on the BW1 surface are always somewhat smaller than those on the BW2. In the same figure, the results of the present (open squares) and previous[22] (filled triangle) experimental measurements as well as the QCT excitation function calculated on the G3 PES are also shown for comparison. The experimental value of (2 ± 1) Å^2 reported in ref 20 for $E_{col} = 1.6$ eV was not included in Figure 4. The experimental cross sections in the energy range $E_{col} = 1.0-1.7$ eV are significantly smaller than those calculated on the new BW PESs. The global accordance between experiment and theory is clearly better if one considers the QCT cross sections of the G3 surface, which are smaller than the BW cross sections by a factor of about two. However, in any case the agreement is only approximate since the G3 cross sections lie outside the experimental error bars for two of the three experimental points. The decrease in $\sigma_R(E_{col})$ observed in the experiments between 1.4 and 1.7 eV was not observed in the calculations. Instead, the cross section on the BW and G3 PESs remains almost constant in the collision energy range $E_{col} = 1-2$ eV.

The lower panel of Figure 4 depicts the calculated excitation functions for the H atom exchange channel of the H + HCl reaction. For the exchange channel the threshold is much higher ($E_0 \approx 0.6$ eV), which reflects the larger reaction barrier for this channel (0.80 eV), and the rise in $\sigma_R(E_{col})$ is much more abrupt than for the abstraction channel. In fact, the exchange reaction cross section grows monotonically and reaches a value of ∼1.5 Å^2 at the highest collision energy investigated ($E_{col} = 2.25$ eV). No experimental cross sections have been reported for this exit channel of the reaction, but the differences between the cross sections calculated on the G3 and BW surfaces are much smaller.

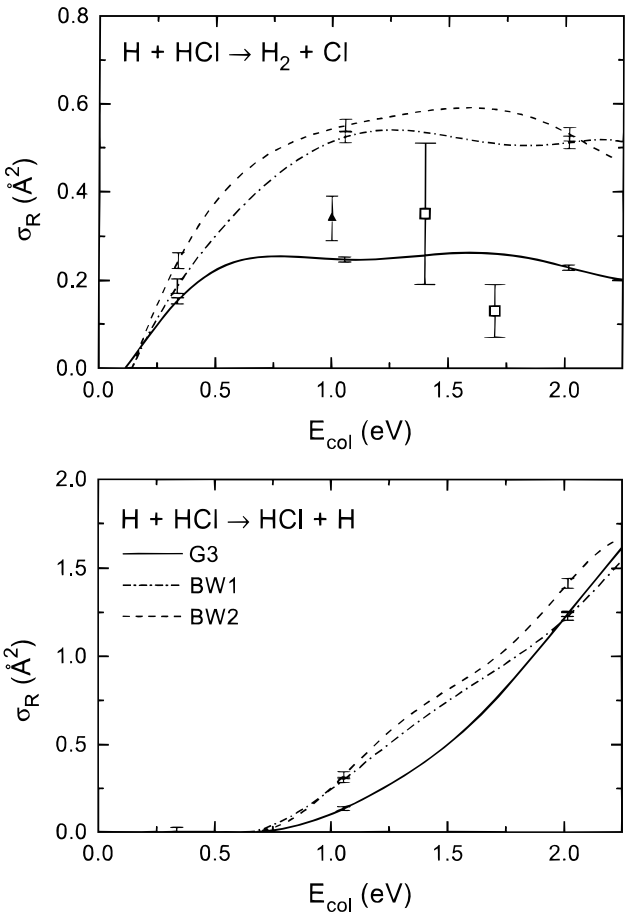

Figure 4. Reaction cross section as a function of collision energy (excitation functions) for the abstraction H + HCl → H_2 + Cl (upper panel) and exchange H + HCl → HCl + H (lower panel) reaction. Calculations were carried out on the G3 (solid line), BW1 (dot−dash line) and BW2 (dashed line) PESs. The triangle is the experimental result of ref 22 while the open squares correspond to the experimental results of the present study. The reaction cross sections were obtained by averaging over the reagent rotational distribution at $T = 300$ K. Notice the different reactivity calculated for the abstraction channel on the G3 PES as compared with that on the BW1 and BW2 PESs.

Figure 5 shows the analogous results for the partially isotopically substituted H + DCl reaction. In this case, the BW cross sections for the abstraction channel, reproduced in the upper panel, reach a broad maximum of 0.4−0.5 Å^2 at $E_{col} \approx 1$ eV, followed by a gentle decline up to the highest energies considered in the calculations. The BW1 cross sections are somewhat smaller than the BW2 ones surely due to the slightly lower barrier of the latter PES. The G3 excitation function,[23] qualitatively similar in shape to the $\sigma_R(E_{col})$ calculated on the BW surfaces, is much smaller in absolute value (by a factor of more than two for $E_{col} > 1$ eV), and is in much better agreement with the experimental abstraction cross sections of Polanyi and co-workers.[21] The cross section for the exchange channel (lower panel of Figure 5) increases from a threshold of about 0.65 eV to a value of approximately 1 Å^2 at $E_{col} = 2.25$ eV. As expected, the BW2 exchange cross sections are slightly larger than the BW1 ones and the values obtained for the two BW PESs are both larger than those obtained on the G3 surface. Reaction

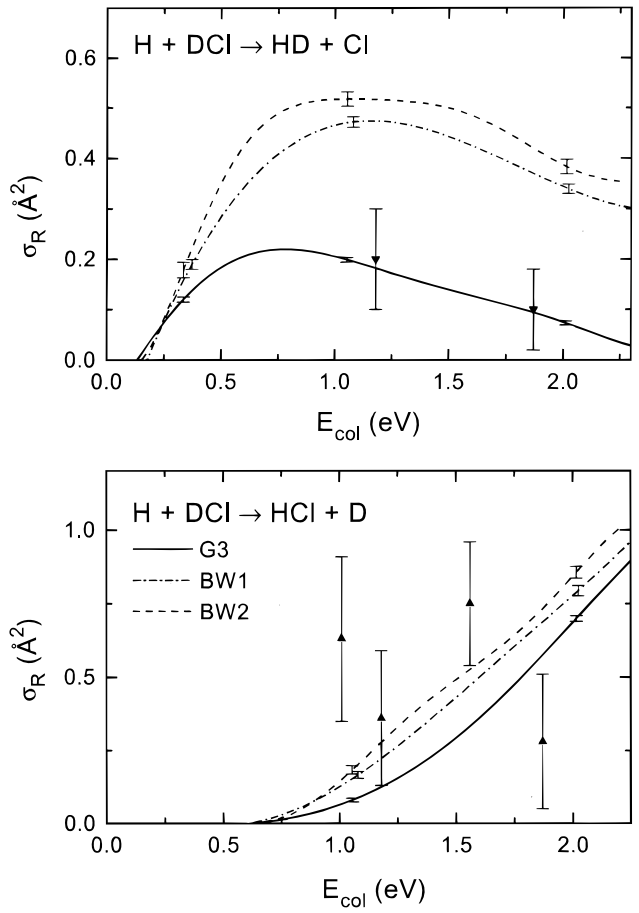

Figure 5. Same as Figure 4 but for the H + DCl reaction. The symbols (up and down triangles) represent experimental results from ref 21.

cross section measurements for the H + DCl → HCl + D exchange reaction were also performed by Polanyi and coworkers[21] with the reported cross section values lying between 0.25 Å^2 and 0.75 Å^2 for the collision energy range considered in the present calculations (see lower part of Figure 5). The experimental values, however, exhibit a great dispersion and, except for the approximate magnitude, are not reproduced by the theoretical calculations on either PES.

Although the new BW surfaces, and in particular the BW2 version, were found especially suited for the simulation of the Cl + H_2/HD low-collision-energy experiments,[17,37] they seem to fail in reproducing the high-energy abstraction cross sections for H + HCl and H + DCl reactions, which are in turn reasonably well justified (vide supra) by QCT calculations on the G3 PES. The large difference in reactivity obtained for the H + HCl and H + DCl abstraction reaction channels on the BW2 and G3 surfaces is surprising at first sight since both PESs have similar transition state regions, corresponding to collinear orientations resembling classical barriers, bending and stretching coordinates.[18]

Some particular features of the BW2 PES were identified as the cause of the success of this PES to account for the experimental Cl + HD excitation functions in strong contrast with the results obtained on the G3 PES when exact QM scattering calculations were carried out.[17] To explain the measured isotopic product branching ratio in the Cl + HD reaction, the existence of an "orienting" van der Waals (vdW) well in the reagent valley of the BW2 was invoked,[17] and the best agreement with the measured Cl + H_2 thermal rate constants could be obtained with a dynamical treatment ac-

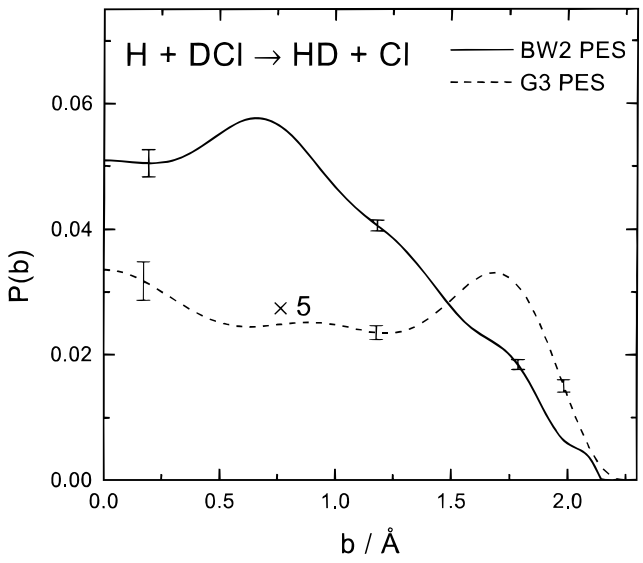

Figure 6. Reaction probability as a function of impact parameter (opacity function) for the H + DCl → HD + Cl reaction at 1.85 eV collision energy. Solid line: results on the BW2 PES. Dashed line: results on the G3 PES. Notice that in the latter case the opacity function has been multiplied by 5 for clarity purposes.

counting in an approximate way for the Cl atom spin−orbit effects by effectively shifting the BW2 barrier upward by 0.036 eV.[37] For the high collision energies at which the experimental H + HCl and H + DCl abstraction cross sections were measured, neither a small variation of the classical barrier for reaction nor a vdW well is expected to affect significantly the outcome of the reactive encounters. The exchange channel of the BW2 surface also exhibits small vdW wells, but the calculated reaction cross sections are not so different from that on the G3 PES, which is a surface without long-range attraction. An inadequacy of the QCT method for these calculations is also unlikely. Far above the reaction threshold, the most common dynamical quantum effects like those associated with tunneling or zero-point energy constraints should be small. Recrossing, which may be important at high collision energies, is generally expected to be smaller in QM calculations than in QCT. Finally, other kinds of quantum effects would be very unlikely for total integral cross sections corresponding to averages over relatively broad distributions of collision energies and internal states. It is somehow surprising that dynamical calculations on the BW2 PES, which is based on high-quality ab initio points and clearly more accurate than any previous PES, yield reaction cross sections for the abstraction channel noticeably larger than the experimental ones. However, nonadiabatic effects, which are not included in the present QCT calculations, may play an important role at sufficiently high collision energies, as it has been shown experimentally (see Figure 2). In addition, it is worth mentioning that spin−orbit coupling effects are not included in the BW2 PES, whereas they are approximately included in the G3, given its partly semiempirical character.

In an attempt to clarify the origin of the contrasting reactivity obtained in the QCT calculations on the G3 and BW PESs, the reaction probability as a function of the impact parameter (opacity function) was analyzed at high collision energy. Figure 6 displays the opacity function, *P(b)*, for the H + DCl → HD + Cl abstraction channel on the G3 and BW2 PESs at E_{col} = 1.85 eV. Notice the great difference in reactivity between the two surfaces (the values of the *P(b)* calculated on the G3 were multiplied by 5). The opacity function calculated on the BW2 PES exhibits a maximum at $b \approx 0.75$ Å and precisely this *b*

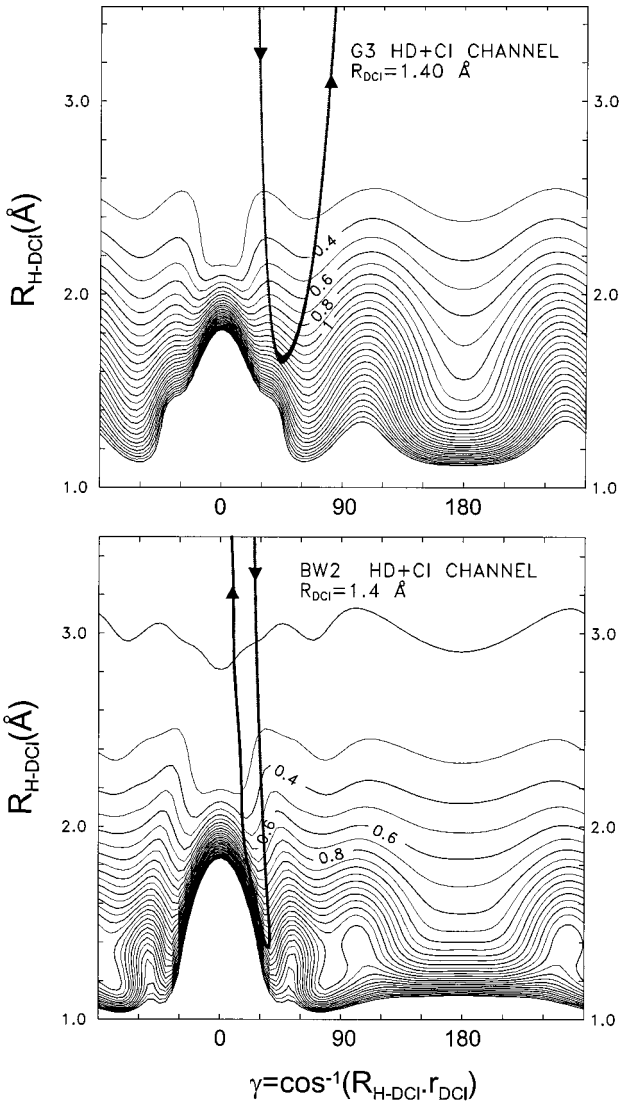

Figure 7. *R*-γ contour plots of the G3 PES (upper panel) and BW2 PES (lower panel). *R* is the distance between the incoming H atom and the center of mass of the DCl molecule. γ is the Jacobi angle between the R_{H-DCl} and R_{DCl} distances, the latter was kept fixed at the value of the saddle point, $R_{DCl} = 1.4$ Å. $\gamma = 0°$ corresponds to the D atom side approach whereas $\gamma = 180°$ correspond to the Cl atom side approach. In both panels a trajectory corresponding to $E_{col} = 1.5$ eV with identical initial conditions has been represented. On the G3 PES the trajectory is nonreactive whereas it is reactive on the BW2 PES. The most salient difference between the topologies of the two PESs consists of the narrow valley on the BW2 PES at angles near $\gamma = 30°$. This valley allows trajectories to reach smaller R_{H-DCl} distances, causing the reactivity due to small impact parameters to be noticeably larger than on the G3 PES.

value corresponds approximately to the center of a shallow minimum in the *P(b)* calculated on the G3 PES. This implies that reactive collisions on the BW2 PES tend to be more "head-on" than those on the G3 surface. Since the main characteristics of the transition state are quite similar on the two PESs, the marked preference for low impact parameters on the BW2 PES, as compared to the G3 one, must be caused by relatively subtle attributes of the PESs.

To gain more insight into the distinct reactive character of these two PESs, we have inspected directly the topological features associated with reactive trajectories leading to the abstraction reaction. For illustrative purposes, we have chosen again the H + DCl system at $E_{col} = 1.85$ eV. Figure 7 shows an *R*-γ contour plot of the two PESs for a fixed DCl internuclear distance of 1.4 Å, which corresponds to the value at the saddle point. In this representation, $\gamma = 0°$ corresponds to the location of the D atom and 180° to that of the Cl atom. As can be seen, there are significant differences in the topology of both surfaces. An analysis of individual trajectories revealed that for the two PESs the cone of acceptance for the abstraction reaction is relatively narrow ($\gamma \approx 0-40°$) and thus reactive collisions have a high degree of collinearity even at this high collision energy. This analysis further showed that the most probable cause of the higher reactivity found on the BW2 PES are the narrow "valleys" in the contour plot centered at $\gamma \approx 30°$, which are absent in the G3 PES. Notice that in this specific region, for a given contour, the *R* value is smaller in the BW2 PES than in the G3. This fact is illustrated in Figure 7 using characteristic trajectories. The two trajectories plotted have identical initial conditions, but that on the G3 PES is actually nonreactive and rebounds after reaching a H−D internuclear distance of ∼1.7 Å. On the other hand, the trajectory on the BW2 surface penetrates deeper into the potential along the narrow valley mentioned above, and after reaching a H−D separation of ∼1.3 Å, finally leads to reaction. Although only one trajectory has been represented in Figure 7 for illustration purposes, a statistical analysis shows that, on average, reactive trajectories leading to the abstraction reaction on the BW2 PES are more penetrating (reaching lower values of R_{H-DCl} distance) than on the G3 PES.

V. Summary and Conclusions

The absolute reactive cross sections measured in the present work for the H + HCl abstraction reaction at collision energies of $E_{col} = 1.4$ and 1.7 eV together with our previous measurement at $E_{col} = 1.0$ eV[22] demonstrate that there is no sharp increase in the H + HCl abstraction reaction cross section in the range $E_{col} = 1.0-1.7$ eV as it was suggested by earlier experiments.[20] The abstraction reaction cross sections of the present work are in a reasonably good agreement with QCT calculations on the G3 PES. Trajectory calculations for the H + HCl and H + DCl reactions on the new BW1 and BW2 potential energy surfaces yielded cross sections for the abstraction pathway, which are too large in comparison with the experimental data as well as with the values obtained on the G3 PES. A closer analysis of the PESs employing *R*-γ contour plots allowed to identify a narrow potential valley centered at $\gamma \approx 30°$ as the cause of the too high reactivity observed for the BW surfaces. For the hydrogen atom exchange channels the reaction cross sections obtained on the BW PES were found to be closer to the cross sections obtained on the G3 PES and compatible with the existing experimental data.[21] Caution should be taken to draw definitive conclusions about the comparative quality of the two surfaces, since the present calculations are purely adiabatic and, moreover, spin−orbit coupling are not included in the construction of the BW PESs.

The experimental studies of the H + HCl reaction further revealed the formation of appreciable amounts of spin−orbit excited Cl*($^2P_{1/2}$) atom products at higher collision energies. The observed collision energy dependence of the Cl* product branching ratio indicates the increasing importance of the nonadiabatic reaction channel H + HCl → H_2 + Cl* with increasing collision energy. However, more work is definitely necessary in order to clarify many aspects still unclear in the dynamics of this fundamental reaction system. On the experimental side comparative studies to investigate the influence of reagent translational excitation and isotopic substitution on the Cl* product branching ratio in the H + DCl reaction as well as

excitation function and reaction threshold measurement for the hydrogen exchange reaction channel are planed for the near future. On the theoretical side multi-surface scattering calculations which take into account the relevant nonadiabatic couplings are clearly needed to assess the role of nonadiabaticity in the H + HCl as well as in the $Cl(^2P_{3/2})/Cl^*(^2P_{1/2})$ + H_2 reactions.[33]

Acknowledgment. We are grateful to Professor H.-J. Werner for providing us with the codes of the BW PESs prior to publication. The Spanish part of this work has been funded by the CICYT of Spain under Grant PB98-0762-C03. The German part of the work has been supported by the Deutsche Forschungsgemeinschaft (DFG). Support in the framework of the German−Spanish scientific exchange program "Acciones Integradas" (HA-1999-0050) and by the Korea Science and Engineering Foundation (Korea−Germany Joint Project 1999-2001) is also gratefully acknowledged.

References and Notes

(1) See, e.g., (a) Allison, T. C.; Mielke, S. L.; Schwenke, D. W.; Lynch, G. C.; Gordon, M. S.; Truhlar D. G. In *Gas-Phase Chemical Reaction Systems: Experiments and Models 100 Years after Max Bodenstein*, Springer Series in Chemical Physics, Vol. 61; Wolfrum, J., Volpp, H.-R., Rannacher, R., Warnatz, J., Eds.; Springer: Heidelberg, 1996; (b) Aoiz, F. J.; Bañares, L.; Herrero, V. J. *J. Chem. Soc., Faraday Trans.* **1998**, *94*, 2483 and references therein.

(2) Bodenstein, M.; Dux, W. *Z. Phys. Chem.* **1913**, *85*, 297.

(3) Laidler, K. J. *Chemical Kinetics*, 3rd ed.; Harper & Row: New York, 1987 and references therein.

(4) Nernst, W. *Z. Elektrochem.* **1918**, *24*, 335.

(5) See, e.g., (a) Clyne, M. A. A.; Stedman, D. H. *Trans. Faraday Soc.* **1966**, *62*, 2164; (b) Westenberg, A. A.; DeHaas, N. *J. Chem. Phys.* **1968**, *48*, 4405; (c) Adusei, G. Y.; Fontijn, A. *J. Phys. Chem.* **1993**, *97*, 1409; (d) Atkinson, R.; Baulch, D. L.; Cox, R. A.; Hampson, R. F., Jr.; Kerr, J. A.; Rossi, M. J.; Troe, J. *J. Phys. Chem. Ref. Data* **1997**, *26*, 521 and references therein.

(6) Leone, S. R.; Moore, C. B. *Chem. Phys. Lett.* **1973**, *19*, 340.

(7) Wilkins, R. L. *J. Chem. Phys.* **1975**, *63*, 534.

(8) Wolfrum J. In *Reactions of Small Transient Species*; Fontijn, A., Clyne, M. A. A., Ed.; Academic Press: New York, 1983.

(9) See, e.g., Kumaran, S. S.; Lim, K. P.; Michael, J. V. *J. Chem. Phys.* **1994**, *101*, 9487; Michael, J. V., in ref 1a.

(10) Mielke, S. L.; Allison, T. C.; Truhlar, D. G.; Schwenke, D. W. *J. Phys. Chem.* **1996**, *100*, 13588.

(11) Aoiz, F. J.; Bañares, L. *J. Phys. Chem.* **1996**, *100*, 18108.

(12) Wang, H.; Thompson, W. H.; Miller, W. H. *J. Chem. Phys.* **1997**, *107*, 7194.

(13) Allison, T. C.; Lynch, G. C.; Truhlar D. G.; Gordon, M. S. *J. Phys. Chem.* **1996** *100*, 13575.

(14) (a) Alagia, M.; Balucani, N.; Cartechini, L.; Casavecchia, P.; van Kleef, E. H.; Volpi, G. C.; Aoiz, F. J.; Bañares, L.; Schwenke, D. W.; Allison, T. C.; Mielke, S. L.; Truhlar, D. G. *Science* **1996**, *73*, 1519; (b) Alagia, M.; Balucani, N.; Cartechini, L.; Casavecchia, P.; Volpi, G. C.; Aoiz, F. J.; Bañares, L.; Allison, T. C.; Mielke S. L.; Truhlar, D. G. *Phys. Chem. Chem. Phys.* **2000**, *2*, 599.

(15) (a) Lee, S.-H.; Lai, L.-H.; Liu, K.; Chang, H. *J. Chem. Phys.* **1999**, *110*, 8229; (b) Lee, S.-H.; Liu, K. *J. Chem. Phys.* **1999**, *111*, 6253.

(16) Kandel, S. A.; Alexander, A. J.; Kim, Z. H.; Zare, R. N.; Aoiz, F. J.; Bañares, L.; Castillo, J. F.; Sáez Rábanos, V. *J. Chem. Phys.* **2000**, *112*, 670.

(17) Skouteris, D.; Manolopoulos, D. E.; Bian, W.; Werner, H.-J.; Lai, L.-H.; Liu, K. *Science* **1999**, *286*, 1713.

(18) Bian, W.; Werner, H.-J. *J. Chem. Phys.* **2000**, *112*, 220.

(19) Wight, C. A.; Magnotta, F.; Leone, S. R. *J. Chem. Phys.* **1984**, *81*, 3951.

(20) Aker, P. M.; Germann, G. J.; Valentini, J. J. *J. Chem. Phys.* **1989**, *90*, 4795.

(21) Barclay, V. J.; Collings, B. A.; Polanyi, J. C.; Wang, J. H. *J. Phys. Chem.* **1991**, *95*, 2921.

(22) Brownsword, R. A.; Kappel, C.; Schmiechen, P.; Upadhaya, H. P.; Volpp, H.-R. *Chem. Phys. Lett.* **1998**, *289*, 241.

(23) Aoiz, F. J.; Herrero, V. J.; Sáez Rábanos, V.; Tanarro, I.; Verdasco, E. *Chem. Phys. Lett.* **1999**, *306*, 179.

(24) Van Veen, G. N. A.; Mohamed, K. A.; Baller, T.; de Vries, A. E. *Chem. Phys.* **1983**, *74*, 261.

(25) Fernández-Alonso, F.; Bean, B. D.; Zare, R. N. *J. Chem. Phys.* **1999**, *111*, 1022.

(26) Baumfalk, R.; Buck, U.; Frischkorn, C.; Nahler, N. H.; Huwel, L. *J. Chem. Phys.* **1999**, *111*, 2595.

(27) Van der Zande, W. J.; Zhang, R.; Zare, R. N.; MacKendrick, K. G.; Valentini, J. J. *J. Phys. Chem.* **1991**, *95*, 8205.

(28) Hilber, G.; Lago, A.; Wallenstein, R. *J. Opt. Soc. Am. B* **1987**, *4*, 1753.

(29) Tonokura, K.; Matsumi, Y.; Kawasaki, M.; Tasaki, S.; Bersohn, R. *J. Chem. Phys.* **1992**, *97*, 8210 and references therein.

(30) Wiese, W. L.; Smith, M. W.; Miles, B. M. *Atomic Transition Probabilities*; Natl. Bur. Stand. Ref. Data Ser., Natl. Bur. Stand. (U.S.) Circ. No 22 (U.S. GPO, Washington, D C, 1969).

(31) Aoiz, F. J.; Herrero, V. J.; Sáez Rábanos, V. *J. Chem. Phys.* **1992**, *97*, 7423.

(32) Aker, P. A.; Valentini, J. J. *Isr. J. Chem.* **1990**, *30*, 157.

(33) Casavecchia, P.; Cartechini, L.; Aoiz, F. J. *Faraday Discuss.* **1999**, *113*, 201.

(34) Bohm, T.; Hanf, A.; Jung, K.-H.; Läuter, A.; Lee, K. W.; Volpp, H.-R. Manuscript in preparation.

(35) Halman, M. *J. Chem. Soc.* **1963**, 2853.

(36) Okabe, H. *The Photochemistry of Small Molecules*; Wiley & Sons: New York, 1978.

(37) Manthe, U.; Bian, W.; Werner, H.-J. *Chem. Phys. Lett.* **1999**, *313*, 647.